High refractive index modification of SiO2 created by femtosecond laser nanostructuring

Barillot, T.; Grojo, D.; Gertsvolf, M.; Lei, S.; Rayner, D. M.; Corkum, P.

Publisher's version / Version de l'éditeur:
https://doi.org/10.1088/0953-4075/43/12/125401
Journal of Physics B: Atomic, Molecular and Optical Physics, 43, 12, pp. 1-5, 2010-06-01

High refractive index modification of SiO_2 created by femtosecond laser nanostructuring

2010 J. Phys. B: At. Mol. Opt. Phys. 43 125401

(http://iopscience.iop.org/0953-4075/43/12/125401)

J. Phys. B: At. Mol. Opt. Phys. **43** (2010) 125401 (5pp) doi:10.1088/0953-4075/43/12/125401

High refractive index modification of SiO_2 created by femtosecond laser nanostructuring

T Barillot[1], D Grojo[1,2], M Gertsvolf[1], S Lei[3], D M Rayner[1] and P B Corkum[1]

[1] Joint Laboratory for Attosecond Science, National Research Council and University of Ottawa, Ottawa, ON K1A0R6, Canada
[2] Laboratoire LP3, UMR6182 CNRS—Universite de la Mediterranee, 163 Avenue de Luminy—C917, 13288 Marseille Cedex 9, France
[3] Kansas State University, 2012 Durland Hall, Manhattan, KS 66506, USA

E-mail: David.Rayner@nrc.ca and Paul.Corkum@nrc.ca

Received 15 March 2010, in final form 6 May 2010
Published 1 June 2010
Online at stacks.iop.org/JPhysB/43/125401

Abstract
By comparing simulations with experiment, we show that the effective refractive index of fused SiO_2 can be locally reduced by $(1.8 \pm 0.2)\%$ by femtosecond laser nanostructuring. We create a microlens of material containing a planar array of nanocracks embedded inside fused silica and probe how it refracts or absorbs light as a function of pulse energy. The self-generated microlens lowers the peak light intensity by deflecting the light around the focus. We obtain the refractive index by simulating the beam transport using the 3D wave equation in conjunction with the measured dimensions of the modified material.

(Some figures in this article are in colour only in the electronic version)

1. Introduction

Light-induced local changes in the refractive index of dielectric solids allow three-dimensional optical devices. Local material densification of amorphous SiO_2 using femtosecond lasers has been widely studied for forming optical elements such as waveguides and photonic circuits [1–3]. However, this relies on a positive refractive index change on the order of 10^{-3}. This raises the fundamental question: what is the maximum refractive index change that can be induced without increasing the scattering or absorption of light? The answer to this question will determine the range of applications of femtosecond laser writing technologies.

A general approach to obtain a large refractive index change is to create alternating regions of material and vacuum as is exploited in photonic crystal optics [4]. As we will see, with appropriate sub-wavelength alternation, scattering is minimal. When a light wave propagates in such structures, its energy resides preferentially in the low-index material and the apparent refractive index is efficiently lowered.

Under certain conditions, femtosecond laser irradiation produces localized, ordered nanostructures of sub-wavelength dimensions in a-SiO_2 [5–8]. Although there is some debate [9], these structures are now thought to consist of nanocracks that are a few nanometres wide [10–13], spaced by the order of $\lambda/2$ where λ is the wavelength of the writing light in the material. They therefore fill the general conditions for large index change proposed above. We have recently communicated the formation of a microlens in a-SiO_2 based on this concept [14]. In this paper, we report more detailed experiments on the optical properties of such lenses, accompanied by a detailed analysis that quantifies the refractive index reduction we achieve at $(1.8 \pm 0.2)\%$. To our knowledge this is the largest refractive index change so far created in SiO_2. The change can be localized on the scale of the laser focus but can also be extended to larger structures by scanning the writing beam [12, 15].

Our work relates to previous studies of planar nanostructures in fused SiO_2 [5, 6]. It has been shown that repeated illumination induces birefringence to the material [15, 16]. Birefringence, in turn, can serve as a diagnostic

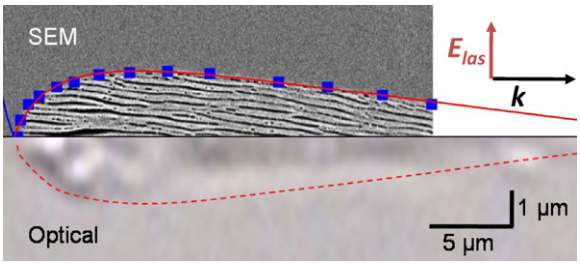

Figure 1. (a) Side-view (optical) and cross-section (SEM) images of the biconvex modified region. The function used to describe the lens shape for modelling the optical properties of the lens (red line) is obtained by fitting the SEM boundary at the blue squares to a log-normal distribution (see the text).

of the material modification [10, 14]. Nanostructures can also control how etchants interact with the sample [17], allowing nanofluidic channels to be fabricated. Taken together, optically produced nanostructures open routes to fabricating a wide variety of advanced devices.

2. Experiments and discussions

2.1. Laser nanostructuring and local refractive index changes

In the experiments, we modify our a-SiO_2 sample (Suprasil I) by applying 10^7 linearly polarized laser pulses ($\lambda_{las} = 800$ nm, $\tau_{las} = 130$ fs, NA $= 0.65$) with 350 nJ energy. The light is focused 75 μm inside the fused silica slabs. The experiments are carried out at a 100 kHz repetition rate, but similar results were also obtained at lower rates (0.4 kHz) showing the absence of accumulation of transient effects on a shot-to-shot basis in our experiment. The experimental procedure for laser writing inside the medium is similar to that described previously in [14]. As shown in figure 1, these conditions lead to well-defined ordered nanostructuring. We will show later that nanostructuring does not introduce linear losses due to scattering. This is of major importance for technological considerations. When writing with lower laser fluences and/or with a low number of pulses, we obtain smooth material changes and/or incomplete nanostructures resulting in very modest index changes. When higher energy densities are deposited, material damages become random [8]. These are inevitably associated with the introduction of dramatic scattering losses.

In figure 1, we show the material change at the focus by optical and scanning electron microscopy (SEM). For SEM observations, the samples are cleaved and etched (1% HF). Previous works have shown that the etched nanostructures obtained for similar conditions consist before etching of ≈8 nm void planar nanocracks ($n_1 = 1$) [10–13]. These are perpendicular to the writing laser polarization and embedded in densified materials ($n_2 > n_0$) [15]. The modification is confined in the pre-focal region which does not exhibit any significant surrounding affected zone. Accordingly, the matter densification between cracks must correspond directly to the amount of material that is removed from void regions. We note the crack-to-crack spacing is large (≅250 nm) with respect to the crack size (≅ 8 nm), so we expect ≅ 3% material densification between cracks.

In this paper we concentrate on the quantitative evaluation of the refractive properties associated with this femtosecond laser-induced nanostructuring. If the refractive index of materials were directly proportional to density and light energy were uniformly distributed in the structure, no net change in the apparent refractive index would be predicted. However, experiments show that the nanostructured materials exhibit noticeable changes. More precisely, when the polarization of incident light is perpendicular to the produced planar nanostructures, the apparent refractive index is greatly reduced [14, 15] because, as we show now, light interacts preferentially with the nanovoid inclusions.

Assuming that the size of all regions is small with respect to the wavelength of incident light (this would be especially true for wavelengths longer than the writing wavelength), the field amplitude can be considered as uniform in each individual void and densified planes. Since a normal component of the electric displacement D must be continuous across surfaces, it must be uniform all over our structured region. The electric field is defined locally as D/ϵ_i, where ϵ_i is the local permittivity. Thus, it is obvious that the light energy is non-uniformly distributed in favour of the low-refractive-index regions. Accordingly, a refractive index reduction which is strongly related to the volume filled by the void cracks is obtained.

Scattering by sub-wavelength features can be described using the Rayleigh formalism and varies with the size of scatters (nanostructures) to the sixth power. We therefore expect that a large index reduction can be achieved with vanishing scattering losses in structures made up of numerous very small cracks. This property can be extended from the infrared to the UV if structuring is performed at the nanometre scale. Our description holds when the electric field is perpendicular to the existing boundaries (p-polarized). For s-polarized light, the refractive properties simply rely on a volume averaging due to the continuity of the electric field across the same boundaries. Refractive index reduction is still expected but to a lesser degree. Also, we expect in accordance with experiments [14] the largest apparent refractive index reduction to arise for planar nanostructuring orthogonal to incident light polarization (p-polarization). Interestingly, it corresponds to the geometry arising spontaneously from our femtosecond laser writing experiment (figure 1). It is therefore of great interest to evaluate the refractive index change that can be achieved precisely.

2.2. Characterizing the refractive properties of the structure

The first step is to demonstrate the large refractive index reduction associated with planar nanostructuring. Figure 1(a) shows that the laser-induced planar nanocracks are confined in a very well defined volume in the focal region which is biconvex by nature. The index change in this volume creates a microlens [14]. We evaluate the refractive index change by measuring the focusing properties of this lens.

We use a low-intensity p-polarized (same as for writing) pulse focused with the same objective at the same location

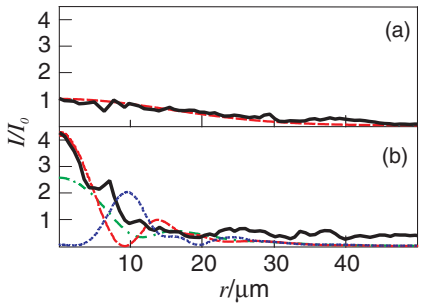

Figure 2. Output beam radial profiles measured at $z_1 = 100\ \mu$m after the focus on (a) fresh and (b) modified material (solid black lines). The calculated beam profile with no microlens is shown as the red dashed curve in (a). Calculated profiles assuming microlens refractive indices of 1.424 (red, _ _ _), 1.412 (green, _.._.._) and 1.4 (blue, . . .) are shown in (b). All intensities are normalized to the peak intensity obtained for unmodified material I_0.

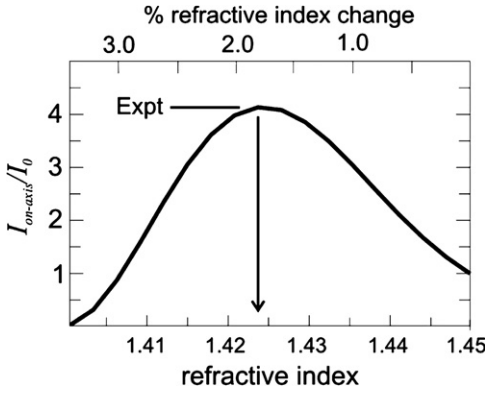

Figure 3. On-axis intensity predicted by modelling beam propagation through the microlens as a function of the effective refractive index of the lens as described in the text. The correspondence of the experimental on-axis intensity to an effective index of 1.424 is shown by the arrow.

as for writing as a probe. Using a collecting objective (NA = 0.75) and a lens ($f = 50$ mm) combination, we image the radial profile of the laser beam at a distance $z_1 = 100\ \mu$m behind the original focus on a CCD. This is in the far field. The experimental procedure is similar to that used in [14]. Figure 2 shows the measured profiles for fresh (a) and modified materials (b). The index change must be large since we observe a strong refraction of the beam. We measure a decrease of the beam size by a factor 5 associated with an increase of the peak intensity by 4.1. This decrease in divergence and the related increase in the on-axis intensity in the far field require that the microlens is negative, implying, through its biconvex shape, a decrease in the refractive index.

We can evaluate the effective refractive index by quantitative modelling of this effect. We solve, using a standard finite-difference approach, the three-dimensional wave equation for an initial Gaussian laser beam focusing inside the medium ($n_0 = 1.45$). The structure is birefringent but our linearly polarized probe beam has its polarization naturally aligned to one of the optical axes. No change in the polarization of the probe beam is expected, allowing us to use the scalar approximation. We concentrate on p-polarized light for which we expect the largest apparent index change. We also make the paraxial approximation that is usually valid for the NA optics used in our experiment [18]. The model takes into account the spatial properties of the lens by fitting its shape by the log-normal distribution (figure 1(a), solid line) $R(z) = -24.4 + 26.5\exp[-(\ln(z/9.43))/5.87]$ where R is the radius of the modified region as a function of the distance z along the optical axis (all distances in μm). This defines a volume in which we can adjust the refractive index to define the microlens. The results of the modelling are compared to experiment in figure 2. Figure 2(a) validates the model by showing that the beam profile calculated for unmodified material matches the experiment well. Figure 2(b) shows that the calculated beam profile is very sensitive to the refractive index of the microlens. The measurement and calculations are in best agreement when the refractive index is set at 1.424.

We find that the on-axis intensity is a sensitive measure of the refractive index. In figure 3 we report on the on-axis intensity predicted by the full numerical n-scan simulation as a function of the microlens refractive index. An increase of the intensity similar to that of the experiment ($\times 4.1$) is only predicted for a limited window of our n-scan (vicinity of $n = 1.424$). According to typical 5% pulse-to-pulse fluctuations in the intensity measurement, we probe a refractive index reduction $\Delta n/n = -(1.8 \pm 0.2)\%$.

This refractive index reduction is in agreement with the value estimated in our earlier communication using the form birefringence relationship for an infinite planar array of nanocracks [14]. The agreement justifies the assumptions made in the earlier paper, reinforcing the link between nanocracking and refractive index change.

Not only the defocusing power of the self-formed lens but also the aberrations associated with its shape grow with the index modulation. This explains the non- monotonous evolution of the on-axis intensity shown in figure 3. When reducing the refractive index in the simulation, the peak intensity first increases due to the negative lens effect of the structure. The lens progressively collimates the beam. However, when we approach $n \approx 1.40$, the phase advance implied through the first interface almost compensates for the curvature of the focused beam ($R_{\text{beam}} \approx 15\ \mu$m). It leads to a nearly plane wave interacting with the conical output interface and it transforms the Gaussian input beam into a beam having a ring structure in its radial profile in the far field as seen in the curves for $n = 1.424$ and 1.412 in figure 2. A decrease of the on-axis intensity is associated with this effect. While our measured beam profiles exhibit some ring structures, these are far less pronounced than those we can predict for a refractive index change exceeding -2%. This predicted feature prevents us from overestimating the index change with our experimental diagnostic.

Having now a firm estimate of the refractive index created by local nanostructuring, one can understand most changes in the transmitted light induced by the modification. Figure 4 shows the far-field characteristics for the weak probe beam interacting with fresh (a) and modified material (b). By translating the beam profiling image plane, we measure the change in divergence due to the lens. We show the

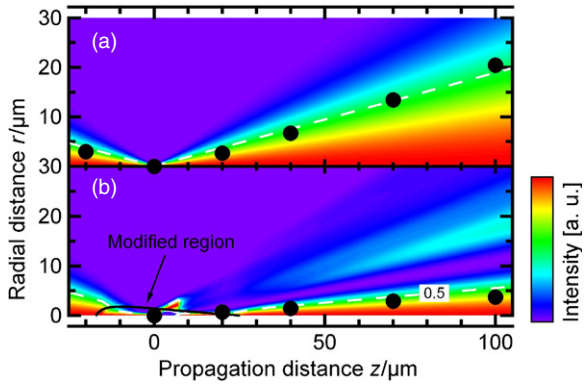

Figure 4. The black circles show the measurement of the beam size (HWHM) as a function of the distance inside fresh (a) and written a-SiO_2 (b). The intensity colour scale image represents calculated intensity beam radial profiles (each normalized to I_{max}). The refractive index of the modified volume is set at 1.424 (1.8% change from bulk).

measurement of the beam half width at half maximum (HWHM) as a function of the distance from the original focus (black circles). This is directly compared with the result of our beam propagation simulation. In figure 4, we incorporate the modified region in the numerical simulation by setting the refractive index at $n = 1.424$ in the indicated region. The images are colour-coded to display the calculated laser intensity $I(r, z) \propto |E(r, z)|^2$. To enhance the presentation, each intensity profile $I(r)$ is normalized to its maximum. The contour (dashed line) corresponds to the calculated z-dependence of the beam size (HWHM). Excellent agreement is observed between experiment and calculations (dashed line). The colour-coded image 4(b) gives insight into the strongly aberrating lens-like behaviour which is at the origin of the measured linear propagation changes.

2.3. Influence of the modifications on nonlinear ionization

According to the lens effect we expect the near-field intensity distribution at the focus to be also significantly affected. This is of great importance since this must influence the beam that creates the nanostructures. Experimentally, one way to monitoring the local peak intensity is to measure the nonlinear absorption of laser pulses as a function of energy. Integrating spheres are used to measure the transmission of individual laser pulses. The energy is adjusted using a half-waveplate and polarizer combination. The experimental details can be found in [19] where similar measurements were performed for fresh material. Figure 5 compares the measurement for fresh material and modified material.

Above the energy of $E_0 = 37$ nJ, we exceed the intensity threshold for multiphoton absorption ($\approx 1.5 \times 10^{13}$ W cm^{-2} inside a-Si0$_2$ [19]). This translates into a significant nonlinear depletion of the pulse. Figure 5 also shows that if a similar measurement is made after writing a structure, an increase in the threshold is observed. Here, the substrate is kept at its original position after writing the structure (10^7 shots) and probed by a small number of probe pulses (< 2000) to ensure that we do not modify the structure during the measurement. Note that the low-intensity

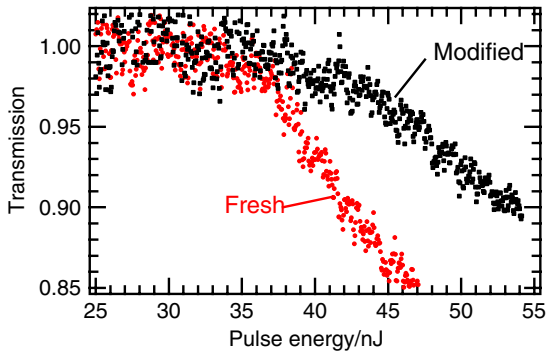

Figure 5. Nonlinear absorption of fresh and modified a-SiO_2 as a function of the laser pulse energy. The modified material has been exposed to 10^7 laser shots at 350 nJ/pulse prior to measuring the absorption.

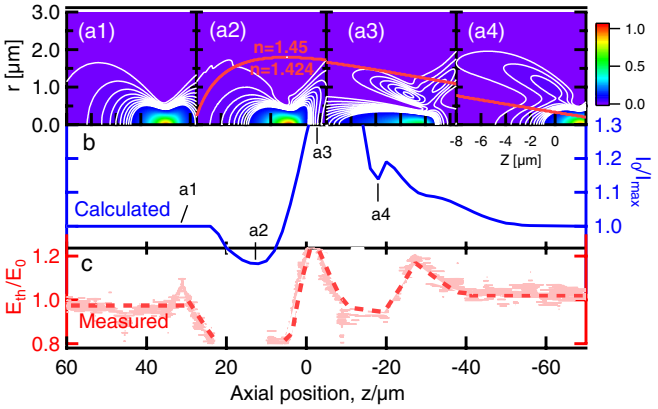

Figure 6. Correlation between the experimental threshold for nonlinear absorption, E_{th}, and the calculated maximum intensity reached in the probe focus, I_{max}, as a function of the axial position, z, of the probe focus with respect to a pre-written microlens. Images (a1)–(a4) show the calculated spatial intensity distribution for beams focused at selected locations inside the structure. Panel (b) shows I_{max}, normalized to the maximum intensity reached in the absence of the microlens, I_0, as a function of z. The variation E_{th} with z is shown in panel (c). E_0 is the threshold in unmodified material.

transmission (corrected for surface reflections) remains near 1 (± 0.02). This shows the very low level of back-scattering or linear losses associated with nanostructuring. However, the microlens formation is accompanied by an increase of the energy required for nonlinear absorption of 20% that we can attribute to a lowering of the peak light intensity by the microlens itself.

We test the correlation between the change in apparent energy threshold for multiphoton absorption and the lensing effect by scanning the beam with respect to the modified region. In figure 6(c), we report the measurement of the energy required for nonlinear absorption (normalized to E_0, the threshold for fresh material) as a function of the focusing distance. For each threshold measurement, a new structure is first formed with the original focus located at $z = 0$. Then, we translate the focusing objective and perform the measurement following the same procedure as above (figure 5). Outside the range $-20\ \mu\text{m} < z < 40\ \mu\text{m}$, that is, when the light is focused outside the lens, we find the same energy required to

initiate ionization ,i.e. the energy threshold for fresh material ($E_{th}/E_0 = 1$). Within the range of modification, we observe large changes in the threshold. Figure 6(a) shows the evolution of intensity spatial distribution $I(r, z)$ at the focus simulated for the same z-scan. Depending on the portions of the beam intercepting the curved front or the sharp tip of the lens, the peak intensity strongly modulates. The inverse of the peak intensity (normalized to the peak intensity if the focus was on fresh material I_0) is plotted in figure 6 as a function of the z-position. While we do not expect the nonlinear absorption threshold measurement to be sensitive to details in local fields, we clearly see that most modulations (figure 6(c)) directly correlate with the calculated peak intensity (figure 6(b)), showing the consistency of our description.

3. Summary and conclusion

Experimentally, using the morphology of the cracked region reported previously [6, 14] we have measured the modification that the nanocracks make to the transmitted light. To determine the refractive index modification quantitatively, we compared the predicted and measured far-field distribution of the transmitted beam. Our simulation uses the 3D wave equation for an initial Gaussian beam focused inside the medium. By tuning the local refractive index in the simulation, we estimate the change to be $-(1.8\pm0.2)\%$ in the experiments. This is achieved without introducing measurable scattering.

A first conclusion is that it is possible to model the transport of probe beams by simply treating our nanostructured region—containing only few tens of nanocracks—(see figure 2) as a region of uniform refractive index. This is of importance since the minimal number of nanostructures making this valid will define a resolution limit in index writing by this approach.

A second conclusion is that the lensing effect associated with refractive index change deflects the writing beam around the focus. We have also shown that the energy required for multiphoton absorption increases as we create the microlens. This reveals the strong interplay between the modifications and the beam that micromachines the material. This observation has implications for modelling multi-pulse experiments.

While we concentrated on a-SiO_2 where nanostructuring is beautifully ordered, a similar lensing effect and subsequent change in nonlinear dissipation were also observed in a wide range of dielectrics under repeated illumination (c-SiO_2, LiF, sapphire and mica [14]). Accordingly, femtosecond laser nanostructuring offers a general way to extend the capacity of direct writing technologies for integrated optics applications.

References

[1] Davis K M, Miura K, Sugimoto N and Hirao K 1996 Writing waveguides in glass with a femtosecond laser *Opt. Lett.* **21** 1729–31

[2] Miura K, Qiu J R, Inouye H, Mitsuyu T and Hirao K 1997 Photowritten optical waveguides in various glasses with ultrashort pulse laser *Appl. Phys. Lett.* **71** 3329–31

[3] Gattass R R and Mazur E 2008 Femtosecond laser micromachining in transparent materials *Nat. Photon.* **2** 219–25

[4] Sakoda K 2005 *Optical Properties of Photonic Crystals* 2nd edn (Berlin: Springer)

[5] Shimotsuma Y, Kazansky P G, Qiu J and Hirao K 2003 Self-organized nanogratings in glass irradiated by ultrashort light pulses *Phys. Rev. Lett.* **91** 247405

[6] Bhardwaj V R, Simova E, Rajeev P P, Hnatovsky C, Taylor R S, Rayner D M and Corkum P B 2006 Optically produced arrays of planar nanostructures inside fused silica *Phys. Rev. Lett.* **96** 057404

[7] Yang W, Bricchi E, Kazansky P G, Bovatsek J and Arai A Y 2006 Self-assembled periodic sub-wavelength structures by femtosecond laser direct writing *Opt. Express* **14** 10117

[8] Hnatovsky C, Taylor R S, Rajeev P P, Simova E, Bhardwaj V R, Rayner D M and Corkum P B 2005 Pulse duration dependence of femtosecond-laser-fabricated nanogratings in fused silica *Appl. Phys. Lett.* **87** 014104

[9] Bellouard Y, Barthel E, Said A A, Dugan M and Bado P 2008 Scanning thermal microscopy and Raman analysis of bulk fused silica exposed to low-energy femtosecond laser pulses *Opt. Express* **16** 19520

[10] Taylor R S, Hnatovsky C, Simova E, Rajeev P P, Rayner D M and Corkurn P B 2007 Femtosecond laser erasing and rewriting of self-organized planar nanocracks in fused silica glass *Opt. Lett.* **32** 2888–90

[11] Hnatovsky C, Taylor R S, Simova E, Rajeev P P, Rayner D M, Bhardwaj V R and Corkum P B 2006 Fabrication of microchannels in glass using focused femtosecond laser radiation and selective chemical etching *Appl. Phys.* A **84** 47

[12] Taylor R S, Hnatovsky C and Simova E 2008 Applications of femtosecond laser induced self-organized planar nanocracks inside fused silica glass *Laser Photon. Rev.* **2** 26–46

[13] Hnatovsky C, Simova E, Rajeev P P, Corkum P B and Taylor R S 2007 Femtosecond laser writing of porous capillaries inside fused silica *Opt. Lett.* **32** 1459

[14] Grojo D, Gertsvolf M, Jean-Ruel H, Lei S, Ramunno L, Rayner D M and Corkum P B 2008 Self-controlled formation of microlenses by optical breakdown inside wide band-gap materials *Appl. Phys. Lett.* **93** 243118

[15] Bricchi E, Klappauf B G and Kazansky P G 2004 Form birefringence and negative index change created by femtosecond direct writing in transparent materials *Opt. Lett.* **29** 119–21

[16] Sudrie L, Franco M, Prade B and Mysyrowicz A 2001 Study of damage in fused silica induced by ultra-short IR laser pulses *Opt. Commun.* **191** 333–9

[17] Hnatovsky C, Taylor R S, Simova E, Bhardwaj V R, Rayner D M and Corkum P B 2005 Polarization-selective etching in femtosecond laser-assisted microfluidic channel fabrication in fused silica *Opt. Lett.* **30** 1867

[18] Sheppard C J 2007 The optics of microscopy *J. Opt. A: Pure Appl. Opt.* **9** S1–6

[19] Rajeev P P, Gertsvolf M, Simova E, Hnatovsky C, Taylor R S, Bhardwaj V R, Rayner D M and Corkum P B 2006 Memory in nonlinear ionization of transparent solids *Phys. Rev. Lett.* **97** 253001